Available online at www.sciencedirect.com
SCIENCE DIRECT®
Comput. Methods Appl. Mech. Engrg. 192 (2003) 509–533
Computer methods in applied mechanics and engineering
www.elsevier.com/locate/cma

A time and space mortar method for coupling linear modal subdomains and non-linear subdomains in explicit structural dynamics

V. Faucher [a], A. Combescure [b,*]

[a] Laboratoire de Mécanique et Technologie, ENS de Cachan, 61, Avenue du Président Wilson, 94340 Cachan, France
[b] Laboratoire de Mécanique des Contacts, INSA, 20, Avenue Albert Einstein, 69621 Villeurbanne Cedex, France

Received 23 January 2002; received in revised form 5 June 2002

Abstract

This paper deals with an extension of dynamic subdomain methods. It relies on time multi-scale algorithms, in the particular case of explicit dynamics. It introduces new opportunities in terms of proper modeling on each subdomain adapted to its effective loading in order to reduce the calculation time of the simulations. Treatment of non-matching meshes and local modal projection methods are thus especially discussed. The efficiency of the method is then illustrated with two large-scale examples.

Keywords: Explicit structural dynamics; Dual Schur domain decomposition method; Multi-time-step method; Non-matching meshes treatment; Modal reduction methods

1. Introduction

The complexity of today's dynamic calculations has generated considerable interest in techniques to accelerate finite element structural analysis. In particular, in the case of explicit dynamics, the large number of time steps necessary to represent impacts correctly and preserve the stability of integration requires improved resolution algorithms. This has led to the emergence of domain decomposition methods, which divide the initial problem into a number of smaller problems—which can be solved at a lesser cost—along with a smaller interface problem which provides all necessary transfers among domains. Among other advantages, these approaches lend themselves quite naturally to efficient computations on parallel machines [1].

Several families of decomposition methods can be identified depending on the way of enforcing the continuity of quantities across the interfaces. One primal method consists of prescribing the continuity of

* Corresponding author.
E-mail addresses: vincent.faucher@lmt.ens-cachan.fr (V. Faucher), alain.combescure@insa-lyon.fr (A. Combescure).

0045-7825/03/$ - see front matter
PII: S0045-7825(02)00549-2

kinematic quantities at the interface a priori and attempting to verify the equilibrium of forces. A preferred alternative is Schur's dual method, in which interface equilibrium is assumed and kinematic continuity is an objective to be verified. There are also mixed methods in which no particular quantity is favored and the interface has a behavior of its own [2]. The dual method, which had already been validated in statics by the FETI method [3], has been extended to dynamics using Newmark's time integration scheme [4]. The latter approach allows a separate time stepping strategy in each subdomain, including a specific treatment of variable time steps which are necessary for efficient and stable calculations in explicit dynamics [5]. This represents the first step towards the particularization of the model in different zones of the structure according to the actual local nature of the solicitations. For example, in impact calculation, the vicinity of the point of impact is subjected to phenomena with a very short time variation, whereas the rest of the structure is more subjected to shaking on a coarser time scale.

The second step of the model optimization process, in terms of enabling efficient calculations with no damaging alteration to the solution, is to allow each subdomain to have its own spatial discretization fineness. This technique enables, on the one hand, a reduction of the number of degrees of freedom per substructure and, on the other hand, an increase in time step in explicit dynamics. For this purpose, one must introduce into the system the capability of managing incompatible meshes at the interfaces. Among the recent methods dedicated to this type of problem [6], we adopted a modified version of the mortar method [7,8].

Finally, in order to reduce the computation time even further, a new approach in transient dynamics consists of applying to subdomains which are subjected only to small perturbations and remain in the linear elastic domain throughout the calculation the same reduction methods often encountered in vibration dynamics [9–11]. Thus, the corresponding subdomains can be advantageously replaced by a modal basis of a much smaller size than the initial problem. This paper aims at defining an efficient way to deal with any kind of reduced model in the framework of multi-domains and multi-time-steps simulations. It does not focus on giving rules to choose the modal basis, which remains to be done by the analyst for each particular calculation.

2. Formalism for multiple domains and multiple time scales with incompatible bonds at the interfaces

2.1. Domain decomposition using Schur's dual method

Once space has been discretized by the finite element method and time by the explicit central difference scheme, the dynamic equilibrium of a structure at each time step can be written in matrix form:

$$\mathbf{M}\ddot{\mathbf{U}}^{n+1} = \mathbf{F}_{\text{ext}} - \mathbf{F}_{\text{int}}(\mathbf{U}^{n+1}) = \mathbf{F}^{n+1}, \tag{2.1.1}$$

where $\mathbf{M}$ is the (diagonal) mass matrix, $\ddot{\mathbf{U}}^{n+1}$ the acceleration at time t_{n+1} and $\mathbf{U}^{n+1}$ the displacement at time t_{n+1} deduced from the known quantities at time t_n.

From the global problem in space, one performs a decomposition of the structure into n substructures. The dynamic equations are solved in each subdomain and the consistency of the global problem is enforced by conditions of continuity at the interfaces, i.e. between two subdomains 1 and 2:

- kinematic continuity: $\mathbf{X}_1 = \mathbf{X}_2$, (2.1.2)
- equilibrium of the interface forces: $\mathbf{F}_1 + \mathbf{F}_2 = 0$. (2.1.3)

In Eq. (2.1.2), $\mathbf{X}_i$ designates a kinematic quantity discretized in time on subdomain i. This can be a displacement, a velocity or an acceleration.

As proved in [4], the choice of discretized velocities to express kinematic continuity leads to a null energy (dissipated or created) at the interface if one couples any Newmark scheme for time integration on each subdomain. It is also shown in [4] that if accelerations or displacements constraints are chosen, there are limitations on the type on Newmark schemes which can be used. We hence write kinematic continuity in terms of velocities by

$$\dot{\mathbf{U}}_1 = \dot{\mathbf{U}}_2. \tag{2.1.4}$$

In Schur's dual method, continuity of the interface forces (2.1.3) is enforced implicitly, whereas kinematic continuity (2.1.4) is verified a posteriori thanks to the use of Lagrange multipliers. One then writes the coupled problem as the minimization of a functional in which one introduces the work associated with the multipliers.

$$\delta \int_0^t \left[\tfrac{1}{2}\dot{\mathbf{U}}_1^{\mathrm{T}}\mathbf{M}_1\dot{\mathbf{U}}_1 + \tfrac{1}{2}\dot{\mathbf{U}}_2^{\mathrm{T}}\mathbf{M}_2\dot{\mathbf{U}}_2 - (\mathbf{F}_{\mathrm{ext}\,1} - \mathbf{F}_{\mathrm{int}\,1})^{\mathrm{T}}\mathbf{U}_1 - (\mathbf{F}_{\mathrm{ext}\,2} - \mathbf{F}_{\mathrm{int}\,2})^{\mathrm{T}}\mathbf{U}_2 - \boldsymbol{\Lambda}^{\mathrm{T}}(\mathbf{C}_1\dot{\mathbf{U}}_1 + \mathbf{C}_2\dot{\mathbf{U}}_2) \right] = 0. \tag{2.1.5}$$

Following the method explained in [4], we now introduce the central difference integration scheme to express $\dot{\mathbf{U}}_i^{n+1}$ in terms of $\ddot{\mathbf{U}}_i^{n+1}$, to obtain the matrix problem to be solved:

$$\begin{bmatrix} \frac{\Delta t}{2}\mathbf{M}_1 & 0 & -\frac{\Delta t}{2}\mathbf{C}_1^{\mathrm{T}} \\ 0 & \frac{\Delta t}{2}\mathbf{M}_2 & -\frac{\Delta t}{2}\mathbf{C}_2^{\mathrm{T}} \\ -\frac{\Delta t}{2}\mathbf{C}_1 & -\frac{\Delta t}{2}\mathbf{C}_2 & 0 \end{bmatrix} \begin{bmatrix} \ddot{\mathbf{U}}_1^{n+1} \\ \ddot{\mathbf{U}}_2^{n+1} \\ \boldsymbol{\Lambda} \end{bmatrix} = \begin{bmatrix} \frac{\Delta t}{2}\mathbf{F}_1^{n+1} \\ \frac{\Delta t}{2}\mathbf{F}_2^{n+1} \\ \mathbf{C}_1{}^{\mathrm{P}}\dot{\mathbf{U}}_1^{n+1} + \mathbf{C}_2{}^{\mathrm{P}}\dot{\mathbf{U}}_2^{n+1} \end{bmatrix}, \tag{2.1.6}$$

where ${}^{\mathrm{P}}\dot{\mathbf{U}}_i^{n+1}$ is the velocity predictor of the central difference scheme.

Matrices $\mathbf{C}_1$ and $\mathbf{C}_2$ carry out the projection of the nodal velocities of subdomains 1 and 2 onto the interface. If the interface nodes coincide, these matrices are Boolean.

In order to solve problem (2.1.5), one splits it into an unconstrained problem (*free*) and a constrained problem (*link*) [4]:

$$\begin{bmatrix} \mathbf{M}_1 & 0 & 0 \\ 0 & \mathbf{M}_2 & 0 \\ 0 & 0 & 0 \end{bmatrix} \begin{bmatrix} \ddot{\mathbf{U}}_{1\,\mathrm{free}}^{n+1} \\ \ddot{\mathbf{U}}_{2\,\mathrm{free}}^{n+1} \\ 0 \end{bmatrix} = \begin{bmatrix} \mathbf{F}_1^{n+1} \\ \mathbf{F}_2^{n+1} \\ 0 \end{bmatrix}, \tag{2.1.7}$$

$$\begin{bmatrix} \frac{\Delta t}{2}\mathbf{M}_1 & 0 & -\frac{\Delta t}{2}\mathbf{C}_1^{\mathrm{T}} \\ 0 & \frac{\Delta t}{2}\mathbf{M}_2 & -\frac{\Delta t}{2}\mathbf{C}_2^{\mathrm{T}} \\ -\frac{\Delta t}{2}\mathbf{C}_1 & -\frac{\Delta t}{2}\mathbf{C}_2 & 0 \end{bmatrix} \begin{bmatrix} \ddot{\mathbf{U}}_{1\,\mathrm{link}}^{n+1} \\ \ddot{\mathbf{U}}_{2\,\mathrm{link}}^{n+1} \\ \boldsymbol{\Lambda} \end{bmatrix} = \begin{bmatrix} 0 \\ 0 \\ \mathbf{C}_1\dot{\mathbf{U}}_{1\,\mathrm{free}}^{n+1} + \mathbf{C}_2\dot{\mathbf{U}}_{2\,\mathrm{free}}^{n+1} \end{bmatrix}, \tag{2.1.8}$$

where $\dot{\mathbf{U}}_{i\,\mathrm{free}}^{n+1} = {}^{\mathrm{P}}\dot{\mathbf{U}}_i^{n+1} + \frac{\Delta t}{2}\ddot{\mathbf{U}}_{i\,\mathrm{free}}^{n+1}$.

The unconstrained problem is equivalent to the resolution of the dynamic equilibrium in each subdomain independently. Then, the calculated accelerations are corrected using the Lagrange multipliers obtained from the constrained problem.

The constrained problem is condensed on the interfaces to yield the Steklov–Poincaré operator $\mathbf{H}$ and the interface problem to be solved:

$$\mathbf{H}\boldsymbol{\Lambda} = -\left(\mathbf{C}_1\dot{\mathbf{U}}^{n+1}_{1\,\mathrm{free}} + \mathbf{C}_2\dot{\mathbf{U}}^{n+1}_{2\,\mathrm{free}}\right), \tag{2.1.9}$$

where

$$\mathbf{H} = \frac{\Delta t}{2}\mathbf{C}_1\mathbf{M}_1^{-1}\mathbf{C}_1^{\mathrm{T}} + \frac{\Delta t}{2}\mathbf{C}_2\mathbf{M}_2^{-1}\mathbf{C}_2^{\mathrm{T}}. \tag{2.1.10}$$

Remark 2.1. Let us observe that combination of Eqs. (2.1.7) and (2.1.8) leads to a non-symmetric form of Eq. (2.1.6). The symmetric form given in Eq. (2.1.6) is obtained if one multiplies both sides of matrix form of Eq. (2.1.7) by $\Delta t/2$. All computations examples presented in the paper use the set of Eqs. (2.1.7) and (2.1.8).

2.2. Multiple time scales in explicit dynamics

Now, one has a different time step for each subdomain 1 and 2 (Fig. 1).

In the case of constant time steps, one being a multiple of the other [4], the dynamic equilibrium on the fine time scale with the separation constrained/unconstrained can be written:

$$\begin{bmatrix} \mathbf{M}_1 & 0 & 0 \\ 0 & \mathbf{M}_2 & 0 \\ 0 & 0 & 0 \end{bmatrix} \begin{bmatrix} \ddot{\mathbf{U}}^n_{1\,\mathrm{free}} \\ \ddot{\mathbf{U}}^j_{2\,\mathrm{free}} \\ 0 \end{bmatrix} = \begin{bmatrix} \mathbf{F}^n_1 \\ \mathbf{F}^j_2 \\ 0 \end{bmatrix}, \tag{2.2.1}$$

$$\begin{bmatrix} m\dfrac{\Delta t_2}{2}\mathbf{M}_1 & 0 & -m\dfrac{\Delta t_2}{2}\mathbf{C}_1^{\mathrm{T}} \\ 0 & \dfrac{\Delta t_2}{2}\mathbf{M}_2 & -\dfrac{\Delta t_2}{2}\mathbf{C}_2^{\mathrm{T}} \\ -m\dfrac{\Delta t_2}{2}\mathbf{C}_1 & -\dfrac{\Delta t_2}{2}\mathbf{C}_2 & 0 \end{bmatrix} \begin{bmatrix} \ddot{\mathbf{U}}^n_{1\,\mathrm{link}} \\ \ddot{\mathbf{U}}^j_{2\,\mathrm{link}} \\ \boldsymbol{\Lambda} \end{bmatrix} = \begin{bmatrix} 0 \\ 0 \\ \mathbf{C}_1\dot{\mathbf{U}}^j_{1\,\mathrm{free}} + \mathbf{C}_2\dot{\mathbf{U}}^j_{2\,\mathrm{free}} \end{bmatrix}. \tag{2.2.2}$$

The unconstrained velocity in subdomain 1 at time t_j is obtained by linear interpolation between times t_0 and t_n:

$$\dot{\mathbf{U}}^j_{1\,\mathrm{free}} = \left(\frac{t_n - t_j}{t_n - t_0}\right)\dot{\mathbf{U}}^0_{1\,\mathrm{free}} + \left(\frac{t_j - t_0}{t_n - t_0}\right)\dot{\mathbf{U}}^n_{1\,\mathrm{free}}. \tag{2.2.3}$$

Then, the condensed problem at the interfaces becomes

$$\frac{\Delta t_2}{2}(m\mathbf{C}_1\mathbf{M}_1^{-1}\mathbf{C}_1^{\mathrm{T}} + \mathbf{C}_2\mathbf{M}_2^{-1}\mathbf{C}_2^{\mathrm{T}}) = -\left(\mathbf{C}_1\dot{\mathbf{U}}^j_{1\,\mathrm{free}} + \mathbf{C}_2\dot{\mathbf{U}}^j_{2\,\mathrm{free}}\right). \tag{2.2.4}$$

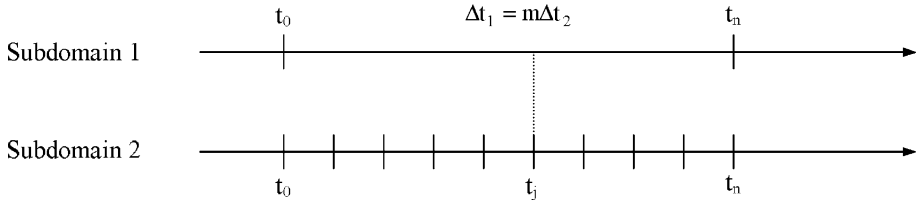

Fig. 1. Constant time steps, one of which is a multiple of the other.

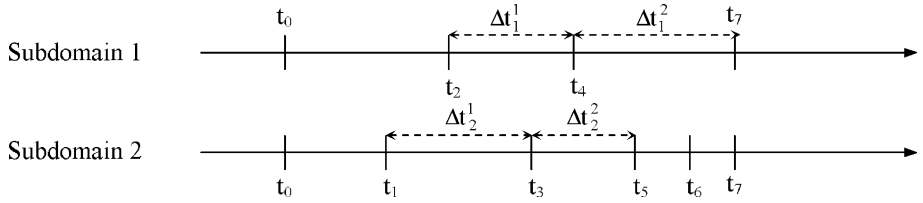

Fig. 2. Arbitrary time steps, varying during the calculation.

In explicit dynamics, for optimum resolution efficiency, it is necessary to adapt the time step to the Courant condition by the sizes of the elements. Therefore, in both subdomains, the time step varies during the calculation (Fig. 2).

This requires adjustments to be made to the multiple time scale coupling as formulated in [5]. For example, the condensed problem at the interfaces at time t_5 becomes

$$\left(\frac{\Delta t_1^2}{2}\mathbf{C}_1\mathbf{M}_1^{-1}\mathbf{C}_1^{\mathrm{T}}+\frac{\Delta t_2^2}{2}\mathbf{C}_2\mathbf{M}_2^{-1}\mathbf{C}_2^{\mathrm{T}}\right)\boldsymbol{\Lambda}^5=-\mathbf{C}_1\dot{\mathbf{U}}_{1\,\mathrm{free}}^5-\mathbf{C}_2\dot{\mathbf{U}}_{2\,\mathrm{free}}^5-\mathbf{C}_1(1-\alpha_1)(\beta_1-1)\frac{\Delta t_2^2}{2}\ddot{\mathbf{U}}_{1\,\mathrm{link}}^4, \qquad (2.2.5)$$

where $\dot{\mathbf{U}}_{1\,\mathrm{free}}^5$ is obtained, as before, by linear interpolation in subdomain 1 between the unconstrained velocities at times t_4 and t_7,

$$\alpha_1=\frac{t_5-t_4}{t_7-t_4},$$

$$\Delta t_1^1=\beta_1\Delta t_1^2.$$

The modifications due to the varying time steps occur on the right-hand side with the appearance of a corrective term function of the constrained acceleration at the previous step for the interpolated subdomain. If the subdomain is not interpolated, $\alpha=1$ and the supplementary term is zero. This also applies if the time step is constant because, then, $\beta=1$.

These results were generalized in [4,5] to k subdomains.

Remark 2.2. The interface energy term $\boldsymbol{\Lambda}^{\mathrm{T}}(\mathbf{C}_1\dot{\mathbf{U}}_1+\mathbf{C}_2\dot{\mathbf{U}}_2)$ is either zero (multi-domain coupling with a single time step) or positive (different time steps). This means that some energy may be dissipated because of linear interpolations of velocities. In any case, the stability of the explicit integration of the system is not affected by the coupling. It is always ensured by the verification of the Courant condition in each subdomain. It is observed in [4,5] on all examples that numerical dissipation at the interface remains less than 1% of the kinetic energy during the calculations.

2.3. Bonding between incompatible meshes

Until now, the kinematic continuity relations prescribed at the interfaces among subdomains were simple nodal relations which coupled all degrees of freedom of an interface node with those of the corresponding nodes in the other subdomains involved. Thus, the $\mathbf{C}_i$ were simple Boolean projection matrices.

Now, these matrices must represent the bonding relations arising from incompatibility. We introduce these new relations during the minimization of the discrete coupled Lagrangian (2.1.5) using, as before, one Lagrange multiplier for each kinematic relation.

Therefore, the concept of interface corresponds to three surfaces:

- 2 physical surfaces: the boundaries of the subdomains in contact,
- 1 virtual surface which supports the Lagrange multipliers.

These three surfaces are physically identical and each one must be discretized:

$$\begin{aligned}
\dot{\mathbf{u}}_1 &= \sum_1^n {}^i\mathbf{N}_1 {}^i\dot{\mathbf{U}}_1 \quad \text{for the boundary of subdomain 1,} \\
\dot{\mathbf{u}}_2 &= \sum_1^m {}^j\mathbf{N}_2 {}^j\dot{\mathbf{U}}_2 \quad \text{for the boundary of subdomain 2,} \\
\boldsymbol{\lambda} &= \sum_1^p {}^k\mathbf{P}^k\boldsymbol{\Lambda} \quad \text{for the support of the Lagrange multipliers,}
\end{aligned} \tag{2.3.1}$$

where n and m are the numbers of degrees of freedom at the interface for subdomains 1 and 2 respectively, p is the number of multipliers introduced, $\{{}^i\mathbf{N}_1\}$ and $\{{}^j\mathbf{N}_2\}$ are the families of shape functions taken at the boundaries of subdomains 1 and 2 respectively, $\{{}^k\mathbf{P}\}$ is the family of shape functions on the support of the multipliers.

The work due to the differential displacements at the interface can be written, in continuous form, as

$$\mathbf{W}_{\text{interf}} = \int_\Gamma \boldsymbol{\lambda}(\dot{\mathbf{u}}_1 - \dot{\mathbf{u}}_2)\,\mathrm{d}s. \tag{2.3.2}$$

Through discretization (2.3.1), this leads to

$$\mathbf{W}_{\text{interf}} = \int_\Gamma \left[\sum_1^p {}^k\mathbf{P}^k\boldsymbol{\Lambda} \left(\sum_1^n {}^i\mathbf{N}_1 {}^i\dot{\mathbf{U}}_1 - \sum_1^m {}^j\mathbf{N}_2 {}^j\dot{\mathbf{U}}_2 \right) \right] \mathrm{d}s. \tag{2.3.3}$$

One expresses the kinematic continuity relations by differentiating the work (2.3.3) with respect to the Lagrange multipliers. One gets two coupling matrices such that

$$\mathbf{C}_1\dot{\mathbf{U}}_1 + \mathbf{C}_2\dot{\mathbf{U}}_2 = 0. \tag{2.3.4}$$

Matrix $\mathbf{C}_I$ contains zeros for all degrees of freedom interior to subdomain I and terms of the form $(-1)^I \int_\Gamma {}^k\mathbf{P}^1\mathbf{N}_I\,\mathrm{d}s$ for the contribution of the 1th degree of freedom of the boundary of subdomain I to the kth continuity relation.

According to this scheme, the whole strategy lies in the choice of the discretization space of the Lagrange multipliers. A criterion is given by the Ladyzenskaia–Babuska–Brezzi condition [12], which specifies that one must not choose too rich a space of multipliers (lest the condensation operator become singular), yet the poorer the space the less well kinematic continuity is verified.

Recently, several authors have proposed discretization methods, particularly for contact–impact problems [13–15]. We are interested in the particular case of the mortar method [7] and in one of its extensions to dual coupling [8]. The former uses the same discretization for the Lagrange multipliers as for one of the subdomains involved. The latter seeks an optimum discretization space in terms of kinematic continuity and inversibility of the condensation operator.

To achieve this optimum expression of bonding, the discretization space of the Lagrange multipliers is taken as the union of the two facing subdomain discretizations, the common nodes being, of course, counted only once (Figs. 3 and 4).

In the optimum case, if $\mathbf{n}$ is the number of nodes on the boundary of subdomain 1, $\mathbf{m}$ is the number of nodes on the boundary of subdomain 2, $\mathbf{c}$ is the number of nodes in common, the number of Lagrange multipliers introduced is

$$\mathbf{p} = \mathbf{n} + \mathbf{m} - \mathbf{c}. \tag{2.3.5}$$

This choice of the space of Lagrange multipliers leads to perfect bonding for first-order finite elements, i.e. zeroing the discretized interface work makes the velocity fields perfectly equal on both sides of the interface [8].

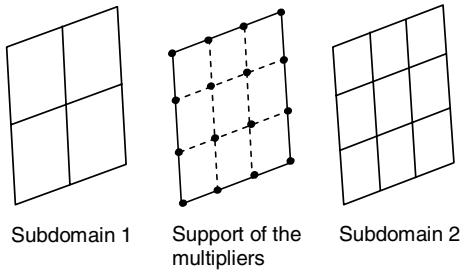

Fig. 3. The mortar method.

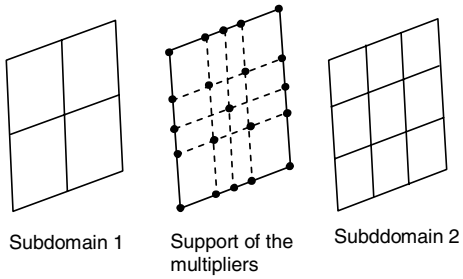

Fig. 4. The optimum method.

It was also proved in [8] that a number of multipliers greater than the optimum makes the condensation operator singular.

Besides, a consequence of perfect bonding in the sense of piecewise affine fields was presented in [8]. The interface velocity field common to the two facing subdomains is logically written on the space of affine functions defined on the set of nodes common to the two meshes. If there are few such common nodes (i.e. three or less in 2D and four or less in 3D), this limits the space of interface velocities, which can result in artificial stiffness of the interface during the calculation. In such a case, one may prefer to use the classical mortar method, which does not present this problem of reducing the dimension of the space of interface fields, even though kinematic continuity is less perfect.

The choice of either method, with its advantages and drawbacks, is a function of the existing discretizations.

Remark 2.3. The proposed ''optimal'' method imposes that the two meshes have at least two common nodes in 2D and three in 3D.

Remark 2.4. The calculation of the coupling matrices depends on the local geometry at the interface. Therefore, these matrices vary as the interface deforms. Of course, during a rigid-body motion of the interface, since the distances between the nodes remain constant, the matrices remain unchanged [8]. Thus, if one is careful to position the incompatible interfaces far away from the zones of high strain gradient, one does not have to reevaluate the coupling terms during the calculation. Locally, the interfaces incur small deformations and one can consider the undeformed and deformed geometries to be the same without adverse consequences.

Remark 2.5. In the case of hierarchical meshes, in which the mesh of one of the subdomains is obtained by subdividing the mesh of the other, the two methods coincide.

3. Modal reduction

3.1. The Ritz method in vibration dynamics

Often, the study of the vibratory behavior of a structure can be greatly simplified by replacing the classical basis of the displacement fields in the structure by a special basis of vectors, usually called the modal basis (Ritz method [11,16]). Classically, this basis is composed of the eigenmodes of vibration of the system, calculated on the free or fixed configuration of the structure at the boundary.

To reduce the number of degrees of freedom, one can select a reduced number of these vibration modes in order, for example, to limit the projection to a subspace corresponding to a given frequency range. To counterbalance truncation effects or to take into account prescribed displacements in the case of modes which are fixed at the boundary of the domain (static correction [16], modal accelerations [17]), one introduces special reduction vectors called static modes [9,10,16].

In all cases, one expresses the projection of the structure's discrete or continuous displacement field onto a finite family of reduction vectors $\{\mathbf{\Phi}_i\}$:

$$\mathbf{U} = \sum_{1}^{N} \mathbf{\Phi}_i \boldsymbol{\alpha}_i = \mathbf{\Phi}\boldsymbol{\alpha}, \tag{3.1.1}$$

where N is the number of modes considered, which is much smaller than the dimension of the initial space of displacements.

3.2. Construction of a reduced model

A number of methods propose to use mode associations in order to reduce the size of a finite element model significantly, taking into account the truncation effects of the basis of eigenvectors. These can be classified into three main families:

1. The static part is given by a series of static responses to a series of unit forces applied sequentially to each degree of freedom at the domain's boundary, the others remaining free.
2. The static part is composed of a series of static responses to a series of unit displacements, each prescribed on one degree of freedom at the boundary, the others being fixed.
3. The static part contains both types of static solutions. One refers to this case as mixed modal synthesis [10].

Remark 3.1. If the structure is not statically stable, the static modes corresponding to unit interface forces must be calculated taking into account the presence of rigid modes which make the stiffness matrix singular. One refers to this process as pseudo-inversion of the stiffness matrix [9,11].

Craig and Bampton's reduction method [18] is the most common method based on static responses to unit boundary displacements. Since the interface degrees of freedom are still visible, it is particularly well suited for primal coupling. In our approach, in which the constraint relations are taken into account in a dual manner, this aspect loses its appeal and both families of methods—forces or displacements at the boundary—are implemented in the same way (see Section 4).

To derive the reduction modes, one splits the displacement $\mathbf{U}$ into boundary degrees of freedom $\mathbf{U}_B$ and interior degrees of freedom $\mathbf{U}_I$. Thus, the system becomes

$$\begin{bmatrix} \mathbf{M}_{BB} & \mathbf{M}_{BI} \\ \mathbf{M}_{IB} & \mathbf{M}_{II} \end{bmatrix} \begin{bmatrix} \ddot{\mathbf{U}}_B \\ \ddot{\mathbf{U}}_I \end{bmatrix} + \begin{bmatrix} \mathbf{K}_{BB} & \mathbf{K}_{BI} \\ \mathbf{K}_{IB} & \mathbf{K}_{II} \end{bmatrix} \begin{bmatrix} \mathbf{U}_B \\ \mathbf{U}_I \end{bmatrix} = \begin{bmatrix} \mathbf{R}_B \\ 0 \end{bmatrix}, \tag{3.2.1}$$

where $\mathbf{R}_B$ is the vector of the reaction forces to the prescribed displacements.

One calculates the quasi-static interior response by static condensation [19]:

$$\mathbf{U}_I = -\mathbf{K}_{II}^{-1}\mathbf{K}_{IB}\mathbf{U}_B. \tag{3.2.2}$$

Thus, one gets the matrix of the static boundary modes, or constrained modes:

$$\mathbf{\Psi}_B = \begin{bmatrix} \mathrm{Id} \\ -\mathbf{K}_{II}^{-1}\mathbf{K}_{IB} \end{bmatrix}. \tag{3.2.3}$$

This matrix describes a subspace of M independent solutions, where M is the number of degrees of freedom of the interface.

To complete the reduction basis, one calculates N normal modes among the $N_T - M$ possible modes (N_T being the total number of degrees of freedom of the system) by solving the vibration problem for the structure fixed at its boundary:

$$(\mathbf{K}_{II} - \omega^2\mathbf{M}_{II})\mathbf{U}_I = 0. \tag{3.2.4}$$

The solutions $\{\mathbf{\Phi}_i\}$ thus obtained form the second part of the reduction basis:

$$\mathbf{\Phi}_I = \begin{bmatrix} 0 \\ \{\mathbf{\Phi}_i\} \end{bmatrix}. \tag{3.2.5}$$

One gets the complete matrix:

$$\mathbf{U} = \begin{bmatrix} \mathrm{Id} & 0 \\ -\mathbf{K}_{II}^{-1}\mathbf{K}_{IB} & \mathbf{\Phi}_I \end{bmatrix} \boldsymbol{\alpha}. \tag{3.2.6}$$

Nevertheless, in both cases, the gain in precision provided by the presence of static modes is offset by two disadvantages which prevent the efficient resolution in an explicit dynamics program.

The first disadvantage is related to the time step. Indeed, if one uses only dynamic modes, it is very easy to control the size of the time step because the highest eigenfrequency present in the system is that of the last mode retained in the basis. If one retains only low-frequency modes, which are the most representative of the global dynamic behavior of the structure, one can expect an increase in the time step by a factor of 50, or even 100, compared to that given by Courant's condition on the finite element model. One could even envisage greater time steps, but the approximations generated by the multiple time scale algorithm could cause problems [4].

The static modes have non-zero projections on the neglected dynamic modes and, therefore, the eigenfrequency of the reduced system is greater than that of the last eigenmode retained. In fact, in practice, it is often very close to the maximum frequency of the initial system, but this cannot be predicted ahead of time without a specific eigenresolution of the reduced model (see Section 3.4).

This is not a major drawback because, even without any gain in terms of time step size, the gain in terms of resolution of the reduced dynamic equilibrium can be sufficient to justify the use of the method.

The second drawback is that, in the presence of many interface degrees of freedom, the number of static solutions introduced into the reduction basis becomes large and affects the efficiency of the resolution of the equilibrium equations. Therefore, one would welcome a further reduction.

At this point, one sees the advantage of being able to select, within a set of reduction vectors, those whose influence is the greatest according to a relevant criterion in order to reduce even further the size of

the reduced model. The appropriate tool used for sorting the vectors is the singular value decomposition [11], which provides the important directions of a subspace. For a reduction matrix $\mathbf{\Phi}$ consisting of N vectors out of the initial N_T degrees of freedom, it takes the following general form:

$$\mathbf{\Phi}_{N_T \times N} = \mathbf{V}_{1\, N_T \times N_T} \mathbf{S}_{N_T \times N} \mathbf{V}^T_{2\, N \times N}, \tag{3.2.7}$$

where the indexes indicate the respective dimensions of the matrices. $\mathbf{S}$ is a diagonal matrix whose diagonal terms are called singular values $\mathbf{V}_1$ and $\mathbf{V}_2$ are matrices of left-hand and right-hand singular vectors respectively.

The families of singular vectors constitute two orthonormal vector bases relatively to a norm, to be defined, which conditions the meaning of the decomposition. The following two norms are commonly proposed in mechanics.

For a displacement field $\mathbf{U}$ which is the quasi-static response to a loading $\mathbf{F}$, the strain energy norm is defined by

$$\|\mathbf{U}\| = \mathbf{U}^T \mathbf{K} \mathbf{U} = \mathbf{F}^T \mathbf{K}^{-1}_{\text{flex}} \mathbf{F}, \tag{3.2.8}$$

where $\mathbf{K}^{-1}_{\text{flex}}$ is the pseudo-inverse of the stiffness matrix in the presence of rigid modes [11].

On the other hand, the kinetic energy norm is given by

$$\|\mathbf{U}\| = \mathbf{U}^T \mathbf{M} \mathbf{U} = \mathbf{F}^T \mathbf{K}^{-1}_{\text{flex}} \mathbf{M} \mathbf{K}^{-1}_{\text{flex}} \mathbf{F}. \tag{3.2.9}$$

Using the kinetic energy norm for basis $\mathbf{V}_2$ and the strain energy norm for basis $\mathbf{V}_1$, for a given kinetic energy, the singular value decomposition leads to the vectors with the highest strain energy in the subspace defined by the columns of $\mathbf{\Phi}$. The vectors whose contribution is the greatest are the left-hand singular vectors associated with the smallest singular values, since the low-strain-energy modes are the most likely to have large amplitudes.

In the case of a reduction by Craig and Bampton's method, one can seek the most important constrained modes using the same reasoning. In this case, the reduced matrices $\mathbf{\Phi}^T \mathbf{M} \mathbf{\Phi}$ and $\mathbf{\Phi}^T \mathbf{K} \mathbf{\Phi}$ are replaced by their equivalents, statically condensed on the interface degrees of freedom [19,20]. With the previous conventions, the basis of vectors can be written:

$$\mathbf{\Psi}_B = \begin{bmatrix} \text{Id} \\ -\mathbf{K}^{-1}_{II} \mathbf{K}_{IB} \end{bmatrix}, \tag{3.2.10}$$

which leads to

$$\begin{aligned} \mathbf{\Psi}^T_B \mathbf{M} \mathbf{\Psi}_B &= \mathbf{M}_{BB} - \mathbf{M}_{BI} \mathbf{K}^{-1}_{II} \mathbf{K}_{IB} - \mathbf{K}_{BI} \mathbf{K}^{-1}_{II} \mathbf{M}_{IB} + \mathbf{K}_{BI} \mathbf{K}^{-1}_{II} \mathbf{M}_{II} \mathbf{K}^{-1}_{II} \mathbf{K}_{IB}, \\ \mathbf{\Psi}^T_B \mathbf{K} \mathbf{\Psi}_B &= \mathbf{K}_{BB} - \mathbf{K}_{BI} \mathbf{K}^{-1}_{II} \mathbf{K}_{IB}. \end{aligned} \tag{3.2.11}$$

3.3. Introduction into the multiple-domain formalism

The structure is discretized using the finite element method and decomposed into two subdomains. Subdomain 1 is subjected to small perturbations throughout the calculation and locally one has a satisfactory reduction basis $\{\mathbf{\Phi}_{1i}\}$ which is assembled into matrix $\mathbf{\Phi}_1$, whose columns are the $\mathbf{n}$ vectors of the$\{\mathbf{\Phi}_{1i}\}$ family. Then, one can write in subdomain 1:

$$\mathbf{U}_1(t) = \sum_1^n \boldsymbol{\alpha}_{1i}(t) \mathbf{\Phi}_{1i} = \mathbf{\Phi}_1 \boldsymbol{\alpha}_1(t) \tag{3.3.1}$$

with $\mathbf{U}_1$ vector of discretized displacements in subdomain 1, $\boldsymbol{\alpha}_1$ vector of modal participations.

Naturally, one also has

$$\begin{aligned}\dot{\mathbf{U}}_1 &= \boldsymbol{\Phi}_1\dot{\boldsymbol{\alpha}}_1,\\ \ddot{\mathbf{U}}_1 &= \boldsymbol{\Phi}_1\ddot{\boldsymbol{\alpha}}_1.\end{aligned} \tag{3.3.2}$$

Thus, one can rewrite the coupled functional which appears in the global minimization (2.1.5) as

$$\begin{aligned}\mathbf{L} &= \int_0^t \Big[\tfrac{1}{2}\dot{\boldsymbol{\alpha}}_1^{\mathrm{T}}\boldsymbol{\Phi}_1^{\mathrm{T}}\mathbf{M}_1\boldsymbol{\Phi}_1\dot{\boldsymbol{\alpha}}_1 + \tfrac{1}{2}\dot{\mathbf{U}}_2^{\mathrm{T}}\mathbf{M}_2\dot{\mathbf{U}}_2 - (\mathbf{F}_{\mathrm{ext}\,1} - \mathbf{K}_1\boldsymbol{\Phi}_1\boldsymbol{\alpha}_1)^{\mathrm{T}}\boldsymbol{\Phi}_1\boldsymbol{\alpha}_1\\ &\qquad - (\mathbf{F}_{\mathrm{ext}\,2} - \mathbf{F}_{\mathrm{int}\,2})^{\mathrm{T}}\mathbf{U}_2 - \boldsymbol{\Lambda}^{\mathrm{T}}(\mathbf{C}_1\boldsymbol{\Phi}_1\dot{\boldsymbol{\alpha}}_1 + \mathbf{C}_2\dot{\mathbf{U}}_2)\Big]\\ &= \int_0^t \Big[\tfrac{1}{2}\dot{\boldsymbol{\alpha}}_1^{\mathrm{T}}\hat{\mathbf{M}}_1\dot{\boldsymbol{\alpha}}_1 + \tfrac{1}{2}\dot{\mathbf{U}}_2^{\mathrm{T}}\mathbf{M}_2\dot{\mathbf{U}}_2 - \hat{\mathbf{F}}_1^{\mathrm{T}}\dot{\boldsymbol{\alpha}}_1 - \mathbf{F}_2^{\mathrm{T}}\dot{\mathbf{U}}_2 - \boldsymbol{\Lambda}^{\mathrm{T}}(\hat{\mathbf{C}}_1\dot{\boldsymbol{\alpha}}_1 + \mathbf{C}_2\dot{\mathbf{U}}_2)\Big]\end{aligned} \tag{3.3.3}$$

with

$$\begin{aligned}\hat{\mathbf{M}}_1 &= \boldsymbol{\Phi}_1^{\mathrm{T}}\mathbf{M}_1\boldsymbol{\Phi}_1,\\ \hat{\mathbf{F}}_1 &= \boldsymbol{\Phi}_1^{\mathrm{T}}\mathbf{F}_{\mathrm{ext}\,1} - \hat{\mathbf{K}}_1\boldsymbol{\alpha}_1,\\ \hat{\mathbf{K}}_1 &= \boldsymbol{\Phi}_1^{\mathrm{T}}\mathbf{K}_1\boldsymbol{\Phi}_1,\\ \hat{\mathbf{C}}_1 &= \mathbf{C}_1\boldsymbol{\Phi}_1,\end{aligned}$$

$\hat{\mathbf{M}}_1$ and $\hat{\mathbf{K}}_1$ being the reduced mass and stiffness matrices of subdomain 1.

This minimization leads to the following matrix system which must be solved after injection of the central difference scheme for coupling with a single time scale:

$$\begin{bmatrix} \dfrac{\Delta t}{2}\hat{\mathbf{M}}_1 & 0 & -\dfrac{\Delta t}{2}\hat{\mathbf{C}}_1^{\mathrm{T}} \\ 0 & \dfrac{\Delta t}{2}\mathbf{M}_2 & -\dfrac{\Delta t}{2}\mathbf{C}_2^{\mathrm{T}} \\ -\dfrac{\Delta t}{2}\hat{\mathbf{C}}_1 & -\dfrac{\Delta t}{2}\mathbf{C}_2 & 0 \end{bmatrix} \begin{bmatrix} \ddot{\boldsymbol{\alpha}}_1^{n+1} \\ \ddot{\mathbf{U}}_2^{n+1} \\ \boldsymbol{\Lambda} \end{bmatrix} = \begin{bmatrix} \dfrac{\Delta t}{2}\hat{\mathbf{F}}_1^{n+1} \\ \dfrac{\Delta t}{2}\mathbf{F}_2^{n+1} \\ \hat{\mathbf{C}}_1{}^{\mathrm{P}}\dot{\boldsymbol{\alpha}}_1^{n+1} + \mathbf{C}_2{}^{\mathrm{P}}\dot{\mathbf{U}}_2^{n+1} \end{bmatrix}. \tag{3.3.4}$$

The structure of this problem is rigorously identical to that which existed prior to projection, given by Eq. (2.1.6). The principle of the resolution and the introduction of the formalism for multiple time scales follow exactly the same steps as above. This also applies to bonding of incompatible meshes, since the same bonding relations can be found through matrices $\hat{\mathbf{C}}_1$ and $\mathbf{C}_2$ written with the modal degrees of freedom of subdomain 1.

Remark 3.2. At the resolution level, the nature of the finite elements involved in the spatial discretization of subdomain 1 disappears to the benefit of modal quantities. Therefore, the calculation program for the reduction modes can use different elements than the fast dynamics program, so long as the same mesh is used at the interface. In our examples, in order to be able to compare the solutions with and without reduction, we will stick to the use of the same elements for the direct and the modal calculations.

Remark 3.3. The reduction basis may contain linearized rigid-body modes. In this case, the projected solution is satisfactory provided that the amplitude of the participation of the rotation modes remains moderate.

For an efficient resolution of the dynamic equilibrium at each time step of an explicit scheme, it is essential that the mass matrix be diagonal. However, classically, in vibration mechanics, the static modes are not orthogonal with one another or with the dynamic modes—whether free or fixed—in the mass sense. Splitting the **n** reduction modes $\{\boldsymbol{\Phi}_{1\,i}\}$ into **p** static modes $\{\boldsymbol{\Phi}_{1\,i}^{\mathrm{S}}\}$ and **q** dynamic modes $\{\boldsymbol{\Phi}_{1\,i}^{\mathrm{D}}\}$ yields reduced matrices with the following structure:

$$\hat{\mathbf{M}}_1 = \left[\begin{array}{c|ccc} \hat{\mathbf{M}}_1^{\mathrm{S}} & \multicolumn{3}{c}{\hat{\mathbf{M}}_1^{\mathrm{SD}}} \\ \hline & \hat{\mathbf{m}}_{11}^{\mathrm{D}} & & 0 \\ \hat{\mathbf{M}}_1^{\mathrm{SD\,T}} & & \ddots & \\ & 0 & & \hat{\mathbf{m}}_{1\mathbf{q}}^{\mathrm{D}} \end{array}\right] \quad \text{and} \quad \hat{\mathbf{K}}_1 = \left[\begin{array}{c|ccc} \hat{\mathbf{K}}_1^{\mathrm{S}} & \multicolumn{3}{c}{0} \\ \hline & \hat{\mathbf{k}}_{11}^{\mathrm{D}} & & 0 \\ 0 & & \ddots & \\ & 0 & & \hat{\mathbf{k}}_{1\mathbf{q}}^{\mathrm{D}} \end{array}\right] \tag{3.3.5}$$

with

$$\begin{aligned} &\hat{\mathbf{M}}_{1ij}^{\mathrm{S}} = \boldsymbol{\Phi}_{1j}^{\mathrm{S\,T}} \mathbf{M}_1 \boldsymbol{\Phi}_{1i}^{\mathrm{S}} \quad \text{and} \quad \hat{\mathbf{K}}_{1ij}^{\mathrm{S}} = \boldsymbol{\Phi}_{1j}^{\mathrm{S\,T}} \mathbf{K}_1 \boldsymbol{\Phi}_{1i}^{\mathrm{S}} \quad \text{for } (i,j) \in [1 \cdots \mathbf{p}]^2, \\ &\hat{\mathbf{M}}_{1ij}^{\mathrm{SD}} = \boldsymbol{\Phi}_{1j}^{\mathrm{S\,T}} \mathbf{M}_1 \boldsymbol{\Phi}_{1i}^{\mathrm{D}} \quad \text{for } (i,j) \in [1 \cdots \mathbf{q}] \times [1 \cdots \mathbf{p}], \\ &\hat{\mathbf{m}}_{1i}^{\mathrm{D}} = \boldsymbol{\Phi}_{1i}^{\mathrm{D\,T}} \mathbf{M}_1 \boldsymbol{\Phi}_{1i}^{\mathrm{D}} \quad \text{and} \quad \hat{\mathbf{k}}_{1i}^{\mathrm{D}} = \boldsymbol{\Phi}_{1i}^{\mathrm{D\,T}} \mathbf{K}_1 \boldsymbol{\Phi}_{1i}^{\mathrm{D}} \quad \text{for } i \in [1 \cdots \mathbf{q}]. \end{aligned}$$

According to the principle of the calculation of the static solutions, the coupling terms between the static and dynamic modes in the stiffness matrix are zero.

Therefore, in order to optimize the explicit resolution of the problem in subdomain 1, it is judicious to orthogonalize the family of reduction vectors completely with respect to the mass matrix.

The first step consists of deducting from the static modes their contribution in the subspace generated by the dynamic modes. This enables one to nullify matrix $\hat{\mathbf{M}}_1^{\mathrm{SD}}$ without altering the remarkable properties of the dynamic modes:

$$\boldsymbol{\Phi}_{1j}^{\mathrm{S}} \leftarrow \boldsymbol{\Phi}_{1j}^{\mathrm{S}} - \sum_{i=1}^{\mathbf{q}} \frac{\boldsymbol{\Phi}_{1j}^{\mathrm{S\,T}} \mathbf{M}_1 \boldsymbol{\Phi}_{1i}^{\mathrm{D}}}{\boldsymbol{\Phi}_{1i}^{\mathrm{D\,T}} \mathbf{M}_1 \boldsymbol{\Phi}_{1i}^{\mathrm{D}}} \boldsymbol{\Phi}_{1i}^{\mathrm{D}} \quad \text{for } j \in [1 \cdots \mathbf{p}]. \tag{3.3.6}$$

This results in the following structure for the projected matrices:

$$\hat{\mathbf{M}}_1 = \left[\begin{array}{c|ccc} \hat{\mathbf{M}}_1^{\mathrm{S}} & \multicolumn{3}{c}{0} \\ \hline & \hat{\mathbf{m}}_{11}^{\mathrm{D}} & & 0 \\ 0 & & \ddots & \\ & 0 & & \hat{\mathbf{m}}_{1\mathbf{q}}^{\mathrm{D}} \end{array}\right] \quad \text{and} \quad \hat{\mathbf{K}}_1 = \left[\begin{array}{c|ccc} \hat{\mathbf{K}}_1^{\mathrm{S}} & \multicolumn{3}{c}{\hat{\mathbf{K}}_1^{\mathrm{SD}}} \\ \hline & \hat{\mathbf{k}}_{11}^{\mathrm{D}} & & 0 \\ \hat{\mathbf{K}}_1^{\mathrm{SD\,T}} & & \ddots & \\ & 0 & & \hat{\mathbf{m}}_{1\mathbf{q}}^{\mathrm{D}} \end{array}\right] \tag{3.3.7}$$

Then, one can orthogonalize the family of modified static modes in order to diagonalize $\hat{\mathbf{M}}_1^{\mathrm{S}}$, which can be done using for instance Schmidt's technique:

$$\begin{aligned} &\boldsymbol{\Phi}_{11}^{\mathrm{S}} \leftarrow \frac{\boldsymbol{\Phi}_{11}^{\mathrm{S}}}{\sqrt{\boldsymbol{\Phi}_{11}^{\mathrm{S\,T}} \mathbf{M}_1 \boldsymbol{\Phi}_{11}^{\mathrm{S}}}}, \\ &\begin{cases} \boldsymbol{\Phi}_{12}^{\mathrm{S}} \leftarrow \boldsymbol{\Phi}_{12}^{\mathrm{S}} - (\boldsymbol{\Phi}_{11}^{\mathrm{S\,T}} \mathbf{M}_1 \boldsymbol{\Phi}_{12}^{\mathrm{S}}) \boldsymbol{\Phi}_{11}^{\mathrm{S}}, \\ \boldsymbol{\Phi}_{12}^{\mathrm{S}} \leftarrow \dfrac{\boldsymbol{\Phi}_{12}^{\mathrm{S}}}{\sqrt{\boldsymbol{\Phi}_{12}^{\mathrm{S\,T}} \mathbf{M}_1 \boldsymbol{\Phi}_{12}^{\mathrm{S}}}}, \end{cases} \\ &\vdots \\ &\begin{cases} \boldsymbol{\Phi}_{1\mathbf{p}}^{\mathrm{S}} \leftarrow \boldsymbol{\Phi}_{1\mathbf{p}}^{\mathrm{S}} - \sum_{1}^{\mathbf{p}-1} (\boldsymbol{\Phi}_{1i}^{\mathrm{S\,T}} \mathbf{M}_1 \boldsymbol{\Phi}_{1\mathbf{p}}^{\mathrm{S}}) \boldsymbol{\Phi}_{1i}^{\mathrm{S}}, \\ \boldsymbol{\Phi}_{1\mathbf{p}}^{\mathrm{S}} \leftarrow \dfrac{\boldsymbol{\Phi}_{1\mathbf{p}}^{\mathrm{S}}}{\sqrt{\boldsymbol{\Phi}_{1\mathbf{p}}^{\mathrm{S\,T}} \mathbf{M}_1 \boldsymbol{\Phi}_{1\mathbf{p}}^{\mathrm{S}}}}. \end{cases} \end{aligned} \tag{3.3.8}$$

The static modes resulting from Schmidt's process are normalized with respect to the mass matrix. Therefore, one proceeds to normalize the dynamic modes as well:

$$\mathbf{\Phi}^{\mathrm{D}}_{1i} \leftarrow \frac{\mathbf{\Phi}^{\mathrm{D}}_{1i}}{\sqrt{\mathbf{\Phi}^{\mathrm{D}\,\mathrm{T}}_{1i}\mathbf{M}_1\mathbf{\Phi}^{\mathrm{D}}_{1i}}}. \tag{3.3.9}$$

One gets the final form for the reduced matrices after projection onto the new modal basis:

$$\hat{\mathbf{M}}_1 = [\mathrm{Id}] \quad \text{and} \quad \hat{\mathbf{K}}_1 = \left[\begin{array}{c|ccc} \hat{\mathbf{K}}^{\mathrm{S}}_1 & \multicolumn{3}{c}{\hat{\mathbf{K}}^{\mathrm{SD}}_1} \\ \hline & \hat{\mathbf{k}}^{\mathrm{D}}_{11} & & 0 \\ \hat{\mathbf{K}}^{\mathrm{SD}\,\mathrm{T}}_1 & & \ddots & \\ & 0 & & \hat{\mathbf{k}}^{\mathrm{D}}_{1\mathbf{q}} \end{array}\right] \tag{3.3.10}$$

The coupling terms of the reduced stiffness matrix between the static and dynamic modes are no longer zero. Nevertheless, the particular form of this matrix must be taken into account both with regard to storage and for optimum efficiency in the calculation of the internal forces for subdomain 1.

Remark 3.4. This method leading to a diagonal mass matrix relies only on linear combinations of the reduction vectors. Therefore, it does not alter the subspace generated by these vectors or the characteristics of the original reduced model.

Remark 3.5. The singular value decomposition introduced in Section 3.2 also yields a set of orthonormal vectors with respect to the mass.

Remark 3.6. The mass diagonalization is only well suited for an explicit time integration scheme. It has no interest with an implicit solver, since the stiffness matrix is still not diagonal.

3.4. Time step evaluation

Using an explicit time integration scheme, a stability condition limits the size of the time step. A default estimator of the limit time step is given by Courant's condition on classical subdomains. For modal ones, Courant's condition still apply but may lead to strongly overestimate the critical time step, since projection (3.3.1) tends to troncate high frequencies within the subdomain. We can compute the exact critical time step from the highest eigenfrequency $\mathbf{f}_{\max}$ of the reduced system on the subdomain, i.e. projected mass and stiffness matrices, $\hat{\mathbf{M}}$ and $\hat{\mathbf{K}}$. Critical time step is finally given by

$$\Delta\mathbf{t}_{\mathrm{crit}} = \frac{1}{\pi\mathbf{f}_{\max}}. \tag{3.4.1}$$

Remark 3.7. If no static modes are used, projected matrices are diagonal and obtaining $\mathbf{f}_{\max}$ is immediate. In the presence of static modes, this frequency must be evaluated from the reduced eigenvalue problem, for example by inverse iteration. The stability time step thus obtained is kept constant during the dynamic calculation, so that its computation is finally costless.

Remark 3.8. We do not discuss in this paper the quality of the modal basis chosen for the analysis. We just suppose that the modes are correctly selected to correctly handle the physical phenomena encountered by the reduced subdomains.

4. Numerical examples

The explicit dynamic calculations were performed using the program EUROPLEXUS developed jointly by the French *Commissariat à l'Energie Atomique* (CEA) and the Joint Research Center of the European Commission. The vibration analyses necessary for the construction of the reduction bases were done using CAST3M from the CEA and *Code_Aster* from *Electricité de France* for the example based on an impact on a nuclear island.

4.1. Bending of a block in 2D plane strain

We first consider a very simple example which demonstrates with a reliable reference solution the good cohabitation betweeen all the numerical methods proposed in this paper. It can be easily reproduced, but because of its simplicity, cannot give any information on the time efficiency of the coupling method.

Let us then consider a rectangular block represented in 2D plane strain, fixed along one of its sides and subjected to a uniformly distributed vertical force on the opposite side (Fig. 5).

The $\mathbf{I}_1\mathbf{I}_2$ interface is incompatible. Only the end nodes of the interface coincide; therefore, we represented it using the mortar method.

Characteristics of the block:

$L = 30$ m
$l = 10$ m
$\rho = 7800\ \mathrm{kg\,m^{-3}}$
$E = 210 \times 10^9\ \mathrm{N\,m^{-2}}$
$v = 0.3$
Linear elastic behavior

Characteristics of the excitation:

Uniform factorized load

$$F(t) = \frac{F_{\max}}{l} S(t)$$

Maximum resultant: $F_{\max} = 3 \times 10^7\ \mathrm{N\,m^{-1}}$
Application function S: heavyside

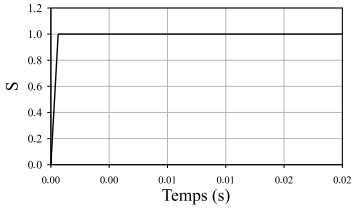

Finite elements: CAR4 quadrangular elements with 4 nodes × 2 d.o.f.s and 4 integration points.

In subdomain 2, we used three different models:

1. The first one was the classical finite element model, which yields 48 degrees of freedom for the subdomain.

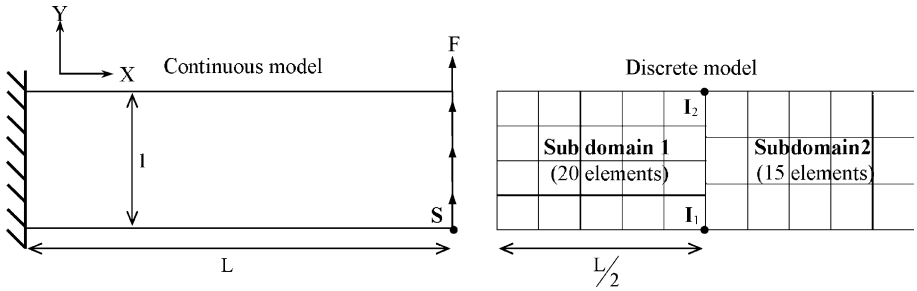

Fig. 5. Continuous and discrete models of the block.

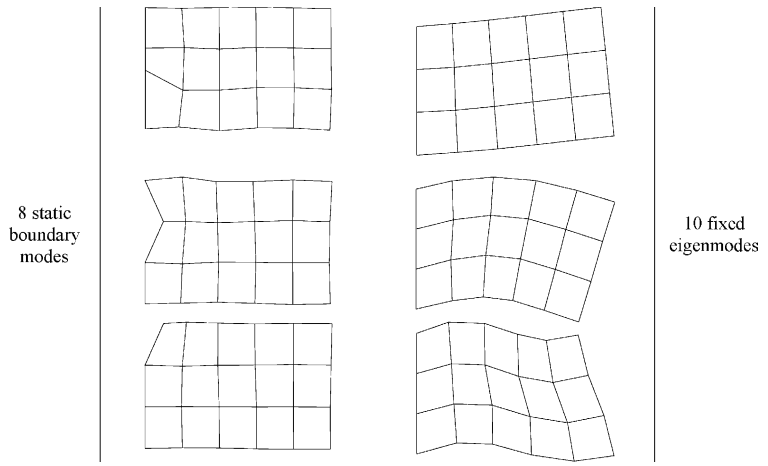

Fig. 6. Craig and Bampton's reduction modes.

2. For the second, we used a reduction basis obtained by Craig and Bampton's method with eight boundary static modes and 10 eigenmodes fixed at the interface, i.e. a total of 18 degrees of freedom (Fig. 6):
3. For the third model, we took 18 free eigenmodes in the reduction basis to yield the same number of degrees of freedom as in the previous case (Fig. 7).

The displacements at point S in the two directions were compared among the three proposed models throughout the simulation. We also show the results of a calculation on the same geometry made without domain decomposition. Among other things, this last calculation enables one to evaluate the quality of the coupling along the incompatible interface (Fig. 8).

Fig. 9 shows the displacements in the X and Y directions respectively for the four models proposed.

First, we observe that the curves representing the two finite element models—single-domain and bi-domain with an incompatible interface—are very similar. This validates the treatment of incompatibility in this case.

Concerning the reduced models, Craig and Bampton's model gave very good results, with a correct maximum amplitude of deformation compared to the single-domain reference and almost no phase shift for the oscillations.

As expected, the free model is the least accurate: the amplitude of the waves is smaller and a phase shift begins to appear at the end of the calculation. Nevertheless, the gain in terms of time step allowed by this

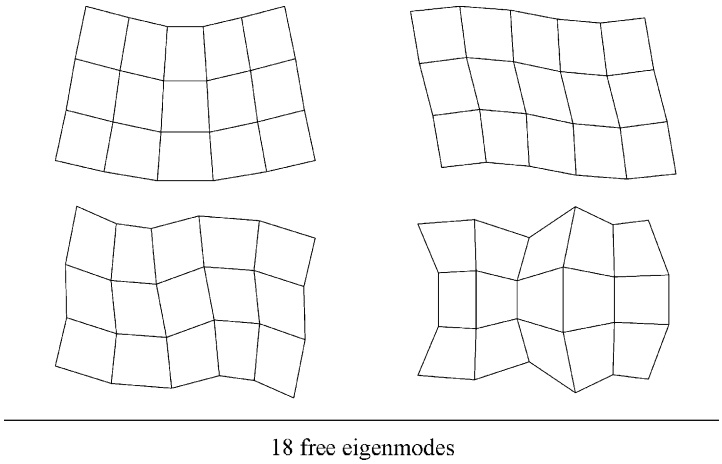

Fig. 7. Free reduction modes.

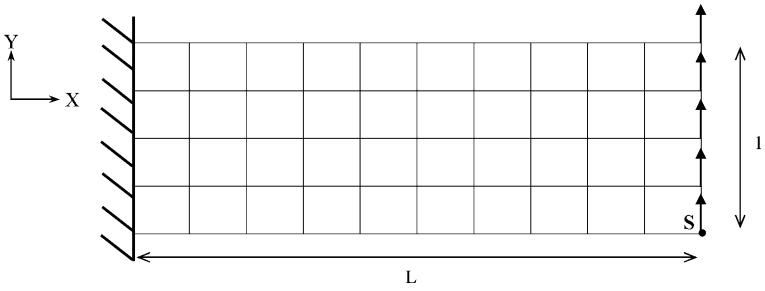

Fig. 8. The single-domain model.

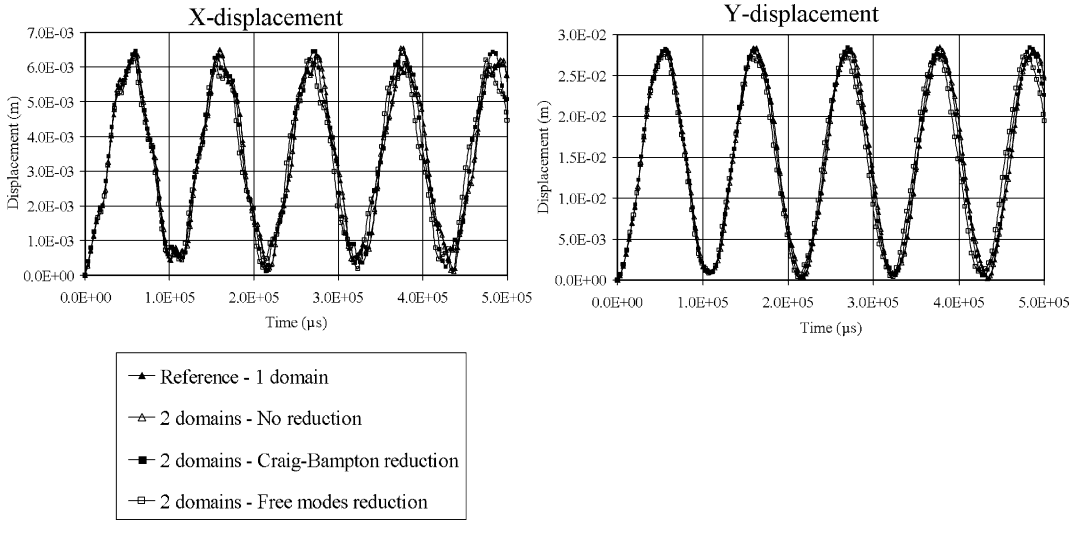

Fig. 9. Displacement at point **S**.

	Single-domain	2 domains	2 domains – Reduction domain 2	
Domain 1	$2.40\text{x}10^{-4}$ s	$2.40\text{x}10^{-4}$ s	$2.40\text{x}10^{-4}$ s	
Domain 2		$2.59\text{x}10^{-4}$ s	$6.22\text{x}10^{-4}$ s (free modes)	$3.10\text{x}10^{-4}$ s (Craig-Bampton)

Fig. 10. Time step sizes in the different configurations.

reduced model is worth mentioning. Here, the stability step size is 6.22×10^{-4} s, whereas for Craig and Bampton's model it was 3.10×10^{-4} s: therefore, the reduced subdomain was calculated only half the time with the pure free mode method. For information, the stability step size on subdomain 2 without reduction is 2.59×10^{-4} s. This confirms that the presence of static modes increases the frequency content of the reduced model significantly and also explains the satisfactory results obtained with this reduction method (Fig. 10).

4.2. Massive 3D structure

Here, the objective was to pinpoint the substantial gains in computation time provided by our multiple-domain calculation method. Therefore, we considered an elaborate structure composed of 2364 8-node brick elements and 4110 nodes with 3 degrees of freedom. The shape of the structure was inspired by a rotor of an aircraft engine which was, of course, highly simplified (Fig. 11).

One of the blades is loaded on the outer face by two uniformly distributed forces: one along Y and the other along Z. The structure is fixed on part of the envelope of the rotor's rear axis, as shown on Fig. 12.

Characteristics of the structure:

Total length: 2 m
Length of a blade: 1 m
$\rho = 7800\ \text{kg m}^{-3}$
$E = 210 \times 10^9\ \text{N m}^{-2}$
$v = 0.3$
Linear elastic behavior

Characteristics of the excitation:

Uniform factorized load along Y:

$$F_Y(t) = \frac{F_{Y\max}}{A} S(t)$$

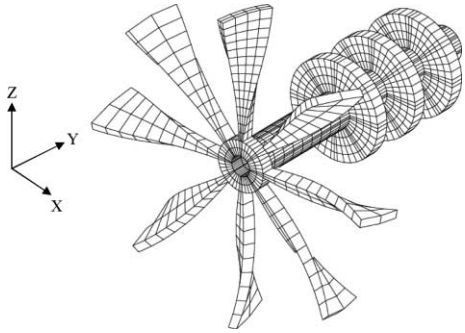

Fig. 11. The mesh of the structure.

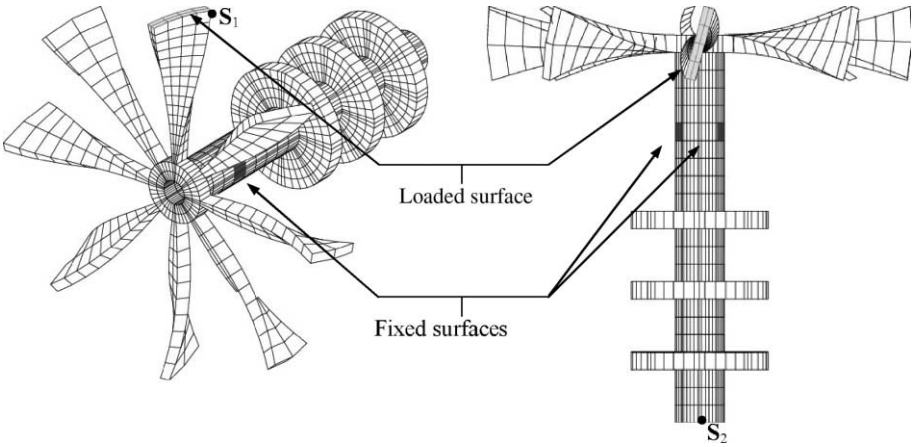

Fig. 12. Loading and boundary conditions.

Maximum resultant: $F_{Y\max} = 15 \times 10^4$ N
Uniform factorized load along Z:

$$F_Z(t) = \frac{F_{Z\max}}{A} S(t)$$

Maximum resultant: $F_{Z\max} = 15 \times 10^4$ N
A: area of the loaded zone (4×10^{-2} m^2)
Application function S: heavyside (same as Example 1)

Finite elements:
CUB8 8-node brick elements with three d.o.f.s and eight integration points.

Remark 4.1. In order to compare the results in subdomain 3 with and without reduction precisely, we did not use elements with reduced integration, although these are popular in explicit dynamics. The reason was that these elements were not available in the calculation code for the reduced subdomain. These elements, once stabilized against hourglass effects, are notoriously more flexible in bending than elements integrated exactly.

We decomposed the structure into three domains:

1. the loaded blade,
2. the disk and the other blades,
3. the rear shaft.

The loaded blade was modeled with a mesh twice as fine as the others in order to improve its bending behavior. This led to an incompatible interface at the base of this blade (Fig. 13).
We proposed two models for subdomain 3:

1. a reference model with classical finite elements,
2. a reduced model with a free basis of free eigenmodes.

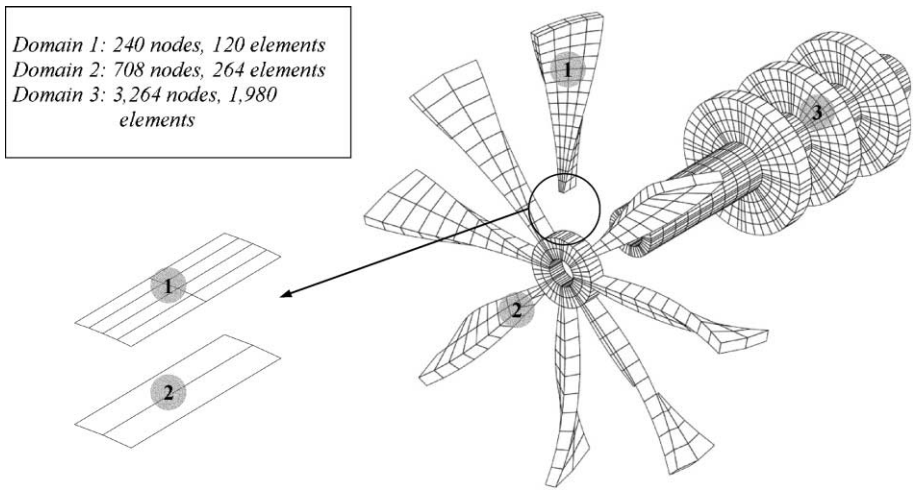

Fig. 13. Decomposition into subdomains.

As we already saw, this reduction method is the most economical one. We aimed especially to verify that, in spite of the reservations already mentioned, it yields satisfactory results, particularly in the frequent cases where only the global movements of the modal subdomain are of interest. In impact problems such as this, the need for precision is acute mostly in the vicinity of the impacted zone.

For the reduction basis, we retained the 50 lowest modes. Since subdomain 3 was composed of 3264 nodes, i.e. 9792 degrees of freedom, this represented a considerable savings in the resolution. Similarly, the time step in the reduced subdomain was 8.03×10^{-4} s, whereas the time step given by the CFL condition on the finite element mesh was 9.68×10^{-7}. Therefore, the reduced subdomain was calculated much less frequently than the initial subdomain (Figs. 14 and 15).

During the simulation, we focused on the displacements of points $\mathbf{S}_1$ and $\mathbf{S}_2$ indicated on Fig. 12 (Fig. 16).

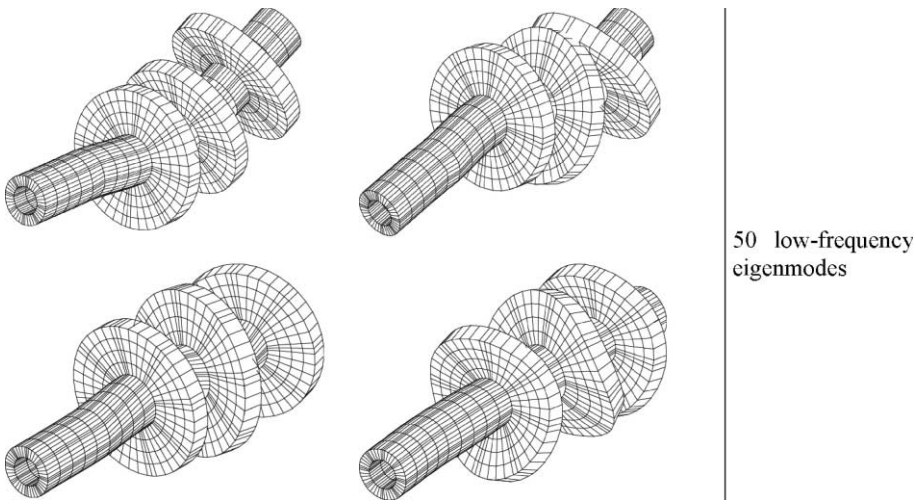

Fig. 14. The reduction modes.

	Without reduction	Reduction on Domain 3
Domain 1	$1.21\text{x}10^{-6}$ s	$1.21\text{x}10^{-6}$ s
Domain 2	$9.68\text{x}10^{-7}$ s	$9.68\text{x}10^{-7}$ s
Domain 3	$9.68\text{x}10^{-7}$ s	$8.03\text{x}10^{-5}$ s

Fig. 15. The time steps in the subdomains.

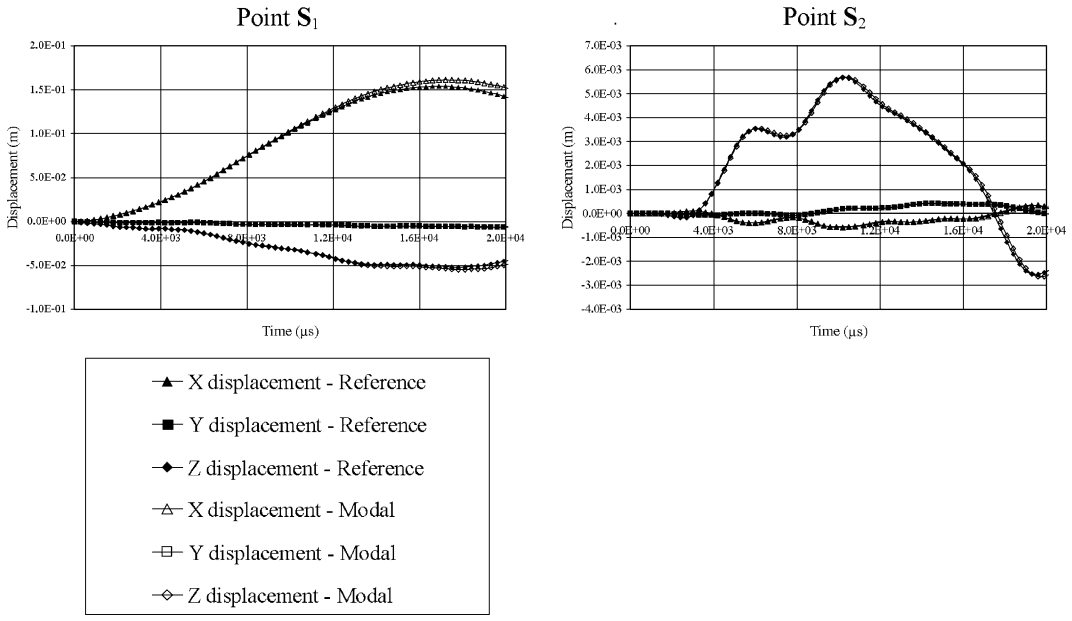

Fig. 16. Displacements at points $\mathbf{S}_1$ and $\mathbf{S}_2$.

The responses in subdomain 3 with and without reduction match very well, which shows how good a reduced model can be if we adjust our expectations accordingly. Furthermore, the gain in terms of computation time is significant, since we have a ratio of 5 for the duration of the calculation with reduction. For information, the multiple-domain calculation already represents a significant gain relative to the single-domain calculation, thanks particularly to the adjustment of the time steps to the local geometry. The single-domain calculation is not represented because, in order to perform such an analysis, we had to give up the refined model of the loaded blade to remove the incompatible interface. The number of nodes is not the same and, besides, the coarse blade is stiffer, which affects the comparison of the results (Fig. 17).

4.3. 3D shell structure

This structure corresponds to the geometry of a nuclear island which consists of a containment vessel housing the core and control structures, surrounded by auxiliary buildings which contain the other parts of the plant. Since the objective of this calculation was to demonstrate the time savings brought about by our approach, the modeling of the behavior of the structure was simplified. The structure is made of linear

Single-domain	3 domains, no reduction	3 domains with reduction
4,630 s	3,383 s	693 s

Fig. 17. Calculation time for 2×10^{-2} s simulation on SGI Origin 2000, sequential processing.

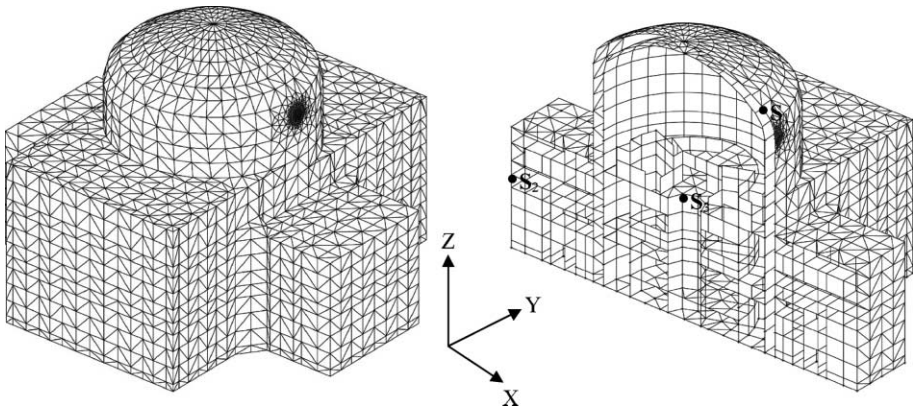

Fig. 18. The mesh of the structure.

elastic concrete, 1.3 m thick. It rests on a system of linear springs acting vertically, which approximately represent the influence of a flexible foundation (Fig. 18).

The mesh was composed of 6871 3-node shell elements and 5806 4-node shell elements, i.e. a total of 6899 nodes with 6 degrees of freedom or 41,394 unknowns.

The structure was subjected to a distribution of loads at the top of the vessel representative of an impact with a military plane (Fig. 19).

Characteristics of the structure:

Height: 75 m
Width: 100 m
$\rho = 7800\ \mathrm{kg\,m^{-3}}$
$E = 210 \times 10^9\ \mathrm{N\,m^{-2}}$
$v = 0.3$
Thickness: 1.3 m
Linear elastic behavior

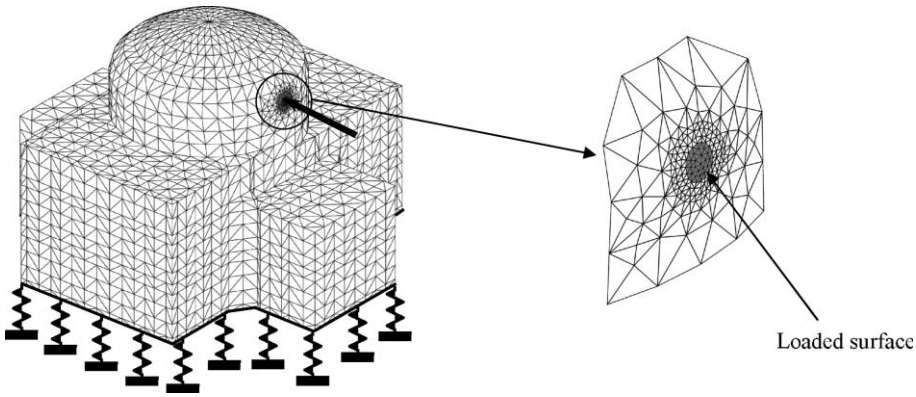

Fig. 19. Loading and boundary conditions.

Characteristics of the excitation:

Pressure: $P(t) = P \times S(t)$
with: $P = 1.15 \times 10^6$ Pa
Application function:

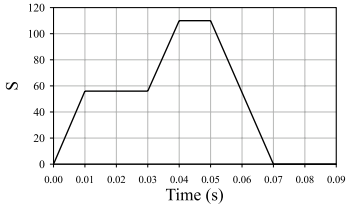

The mesh was refined in the vicinity of the impact zone and preliminary calculations on a vessel modeled using an elastic–plastic concrete law proved that the extent of the plastic zone remains small. This led to the following decomposition into subdomains (Fig. 20).

Again, we proposed two models for subdomain 1:

1. a reference model with classical finite elements,
2. a reduced model with a Craig and Bampton reduction basis. The small number of static modes (84) did not call for a decomposition into singular values for a second level of reduction.

We associated the 84 static modes with the 150 vibration modes fixed on the interface between domains 1 and 3 which had the lowest eigenfrequencies. The number of unknowns in subdomain 1 went down from 40,338 to 234. Furthermore, according to the table in Fig. 21, the stability step increased by a factor 5 thanks to the reduction (Fig. 22).

Let us focus on the displacements in the three directions of points $\mathbf{S}_1$, $\mathbf{S}_2$ and $\mathbf{S}_3$ represented on Fig. 23.

The agreement between the responses with and without reduction is satisfactory both in amplitude and in phase for points $\mathbf{S}_1$ and $\mathbf{S}_2$ located on the external envelope of the island. Concerning point $\mathbf{S}_3$ located at the level of the core, the response after reduction does not properly reproduce the amplitude response of the

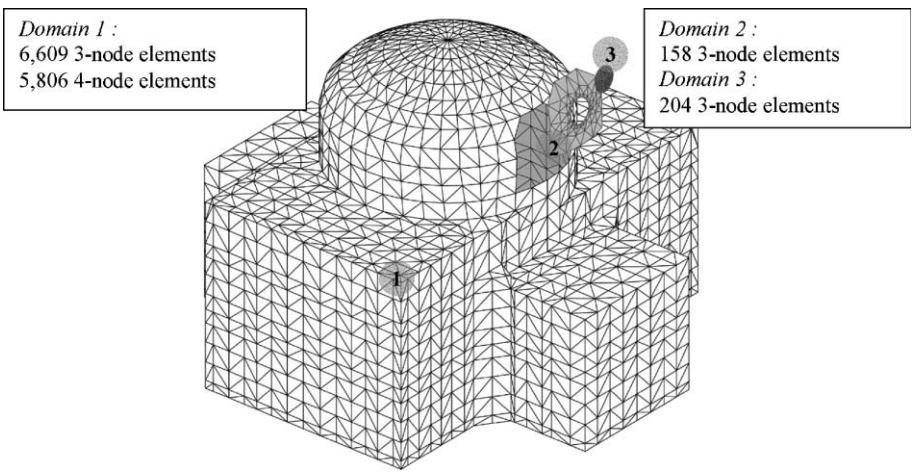

Fig. 20. Decomposition into subdomains.

	Domain 1	Domain 2	Domain 3
Without reduction	$2.60\text{x}10^{-5}$ s	$4.70\text{x}10^{-6}$ s	$2.42\text{x}10^{-6}$ s
With reduction	$1.32\text{x}10^{-4}$ s	$4.70\text{x}10^{-6}$ s	$2.42\text{x}10^{-6}$ s

Fig. 21. Time steps in the subdomains.

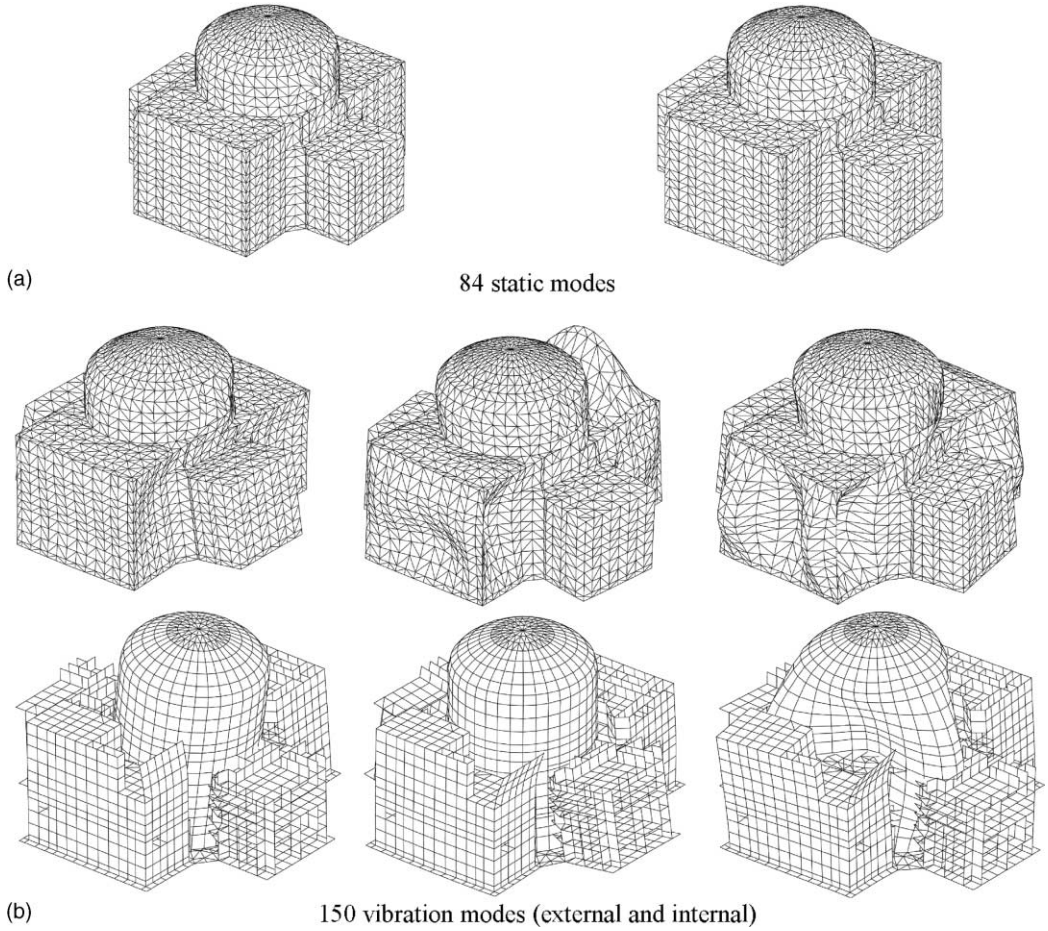

Fig. 22. Craig and Bampton reduction modes.

reference calculation, particularly in the vertical direction. This probably means that the heaving mode of the internal vessel is not represented in the basis because its frequency is higher than the cutoff frequency retained. Therefore, in this case, the vibration model must be improved. In general, the choice of the modes is a crucial point in achieving a quality response after reduction and it is highly dependent on the responses one wishes to measure. For example, in our case, one must verify the presence in the reduction basis of the modes which contribute the most to the displacement of the internal vessel if this is where we wish to measure a representative displacement. Of course, an improvement of the vibration model has limited consequences on the cost of the subsequent calculations because a few additional modes affect the resolution of the free problem on the reduced subdomain only slightly and the corresponding computation time is negligible.

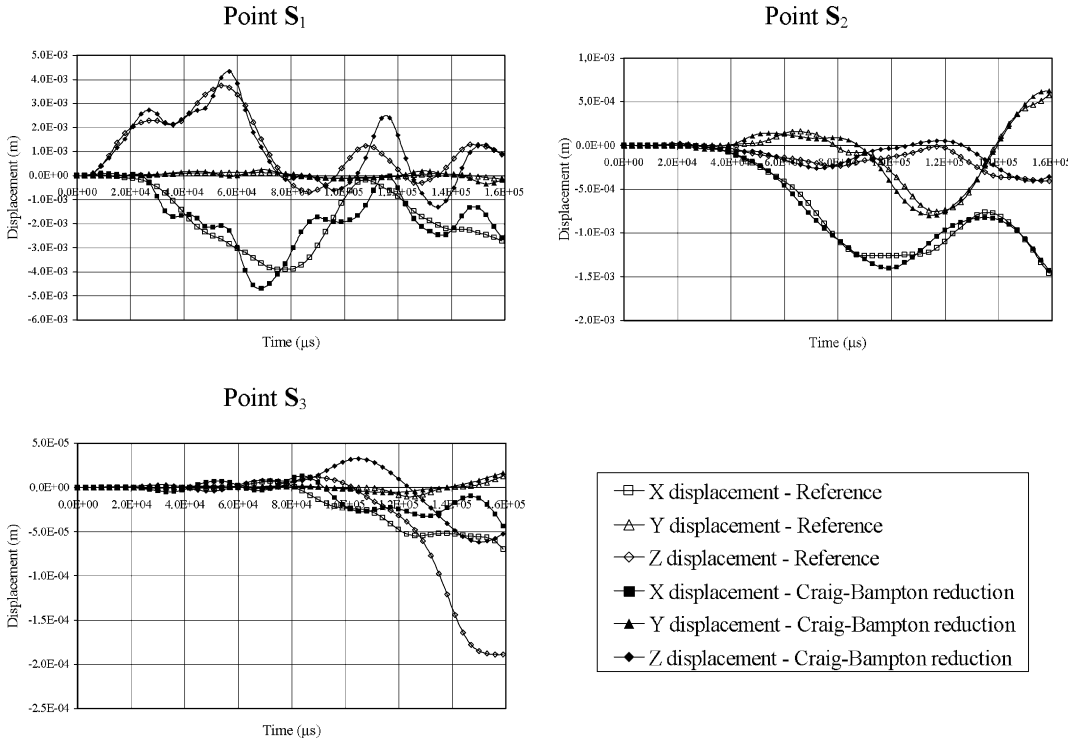

Fig. 23. Displacements at points $\mathbf{S}_1$, $\mathbf{S}_2$ and $\mathbf{S}_3$.

Reference without reduction	Craig-Bampton reduction	Single-domain
3,766 s	853 s	22,722 s

Fig. 24. Calculation time for 160 ms simulation on SGI Origin 2000, sequential processing.

As far as the gain of time for the explicit resolution of the impact problem is concerned, the reduction provides a significant savings since there is a ratio greater than 4 between the calculation times with and without reduction. If we compare this processing time with that obtained with classical tools, i.e. without decomposition into subdomains, the ratio even exceeds 30. Of course, one must add, in the reduction case, the time of the extraction of the modes, which is around 6000 s. Then, we can see that modal projection becomes very attractive as the number of dynamic calculations with an identical modal basis increases, for example if one wants to test several load cases. It also allows one to increase the simulation time in order to analyze phenomena which occur on a time scale greater than that normally allowed by explicit calculations (Fig. 24).

5. Conclusion

We started from a multi-domain, multi-time-step formalism which can handle the mesh incompatibilities between subdomains while preserving the stability of the integration of the equilibrium equations using an explicit scheme. We extended this model adaptation method to local geometries and solicitations using

reduction methods. Several sets of reduction vectors were tested and their advantages and drawbacks, from the point of view of the efficiency of the explicit resolution, were identified. Similarly, we were careful in adapting the structure of classical reduction bases to the constraints arising from this principle of time integration, particularly in order to preserve the diagonal character of the mass. The quality of the response with the reduction technique and the significant gains which can be achieved in terms of calculation time have been demonstrated through two large-scale examples.

Choosing a domain decomposition, the subdomains to reduce and the modes to select in the reduction basis remain the major difficulties to overcome to obtain good results with our approach. This was however not the purpose of this paper. It was dedicated to the analysis of the possible coupling between modal subdomains and direct subdomains and of its efficiency in the framework of explicit dynamics. Appropriate methods to select modes shall be presented later.

References

[1] L. Champaney, D. Dureisseix, Calcul de structures et parallélisme: un bilan et quelques développements récents, Méc. Ind. 1 (2000) 43–60.
[2] P. Ladevéze, Mécanique Non-linéaire des Structures—Nouvelle Approche et Méthodes de Calcul Non-incrémentales, Hermés, Paris, 1996.
[3] C. Farhat, F.X. Roux, Implicit parallel processing in structural mechanics, Comput. Mech. Adv. 2 (1994).
[4] A. Gravouil, A. Combescure, Multi-time-step explicit–implicit method for non-linear structural dynamics, Int. J. Numer. Met. Engrg. 50 (2001) 199–225.
[5] N. Bousquet, EUROPLEXUS—Une méthode de décomposition de domaines en dynamique explicite. Rapport interne no. 243, LMT-Cachan, 2000.
[6] K.C. Park, C.A. Felippa, A variational principle for the formulation of partitioned structural systems, Int. J. Numer. Met. Engrg. 47 (2000) 395–418.
[7] C. Bernardi, Y. Maday, A.T. Patera, A new non-conforming approach to domain decomposition; the mortar element method, in: Non-linear partial differential equations and their applications, Collége de France seminar, Pitman, 1990.
[8] B. Herry, L. Di Valentin, A. Combescure, An approach to the connections between subdomains with nonmatching meshes for transient mechanical analysis, Int. J. Numer. Met. Engrg. 55 (2002) 973–1003.
[9] M. Géradin, D. Rixen, Théorie des Vibrations. Application á la Dynamique des Structures, Masson, Paris, 1993.
[10] R.J. Gibert, Vibrations des Structures. Interactions avec les Fluides, Sources D'excitation Aléatoires, Editions Eyrolles, Paris, 1988.
[11] E. Balmés, Modéles expérimentaux complets et modéles réduits en dynamique des structures, Mémoire d'habilitation á diriger des recherches, Université Paris VI, 1997.
[12] F. Brezzi, M. Fortin, Mixed and Hybrid Finite Elements Methods, Springer Verlag, 1991.
[13] L. Champaney, J.Y. Cognard, P. Ladevéze, Modular analysis of assemblages of three dimensional structures with unilateral contact conditions, Comput. Struct. 19 (1999) 249–262.
[14] P. Hild, Numerical implementation of two nonconforming finite element methods for unilateral contact, Comput. Meth. Appl. Mech. Engrg. 184 (2000) 99–123.
[15] P. Coorevits, P. Hild, J.P. Pelle, A posteriori error estimation for unilateral contact with matching and non-matching meshes, Comput. Meth. Appl. Mech. Engrg. 186 (2000) 65–83.
[16] R. Ohayon, C. Soize, Structural Acoustics and Vibrations. Mechanical Models, Variational Formulations and Discretization, Academic Press, 1998.
[17] L.J.W.S. Rayleigh, Theory of Sound, Dover Publications, New York, 1945.
[18] R. Craig, M. Bampton, Coupling of substructures for dynamic analysis, AIAA J. 4 (1961–1962) 265–271, 332–345.
[19] R.J. Guyan, Reduction of stiffness and mass matrices, AIAA J. 3 (2) (1965) 380.
[20] B.M. Irons, Structural eigenvalues problems: elimination of unwanted variables, AIAA J. 3 (5) (1965) 961–962.